Heavy quark transport in heavy ion collisions at energies available at the BNL Relativistic Heavy Ion Collider and at the CERN Large Hadron Collider within the UrQMD hybrid model

Thomas Lang,[1] Hendrik van Hees,[1,2] Gabriele Inghirami,[1,2,*] Jan Steinheimer,[1,2,3] and Marcus Bleicher[1,2]
[1]*Frankfurt Institute for Advanced Studies (FIAS), Ruth-Moufang-Str. 1, 60438 Frankfurt am Main, Germany*
[2]*Institut für Theoretische Physik, Johann Wolfgang Goethe-Universität, Max-von-Laue-Str. 1, 60438 Frankfurt am Main, Germany*
[3]*Lawrence Berkeley National Laboratory, 1 Cyclotron Road, Berkeley, California 94720, USA*
(Received 2 July 2015; published 5 January 2016)

We implement a Langevin approach for the transport of heavy quarks in the ultrarelativistic quantum molecular dynamics (UrQMD) hybrid model, which uses the transport model UrQMD to determine realistic initial conditions for the hydrodynamical evolution of quark gluon plasma and heavy charm and bottom quarks. It provides a realistic description of the background medium for the evolution of relativistic heavy ion collisions. The diffusion of heavy quarks is simulated with a relativistic Langevin approach, using two sets of drag and diffusion coefficients, one based on a T-matrix approach and one based on a resonance model for elastic scattering of heavy quarks within the medium. In the case of the resonance model we investigate the effects of different decoupling temperatures of heavy quarks from the medium, ranging between 130 and 180 MeV. We present calculations of the nuclear modification factor R_{AA}, as well as of the elliptic flow v_2 in Au + Au collisions at $\sqrt{s_{NN}} = 200$ GeV and Pb + Pb collisions at $\sqrt{s_{NN}} = 2.76$ TeV. To make our results comparable to experimental data at the Relativistic Heavy Ion Collider (RHIC) and Large Hadron Collider (LHC), we implement a Peterson fragmentation and a quark coalescence approach followed by semileptonic decay of the D and B mesons to electrons. We find that our results strongly depend on the decoupling temperature and the hadronization mechanism. At a decoupling temperature of 130 MeV we reach a good agreement with the measurements at both the RHIC and the LHC energies simultaneously for the elliptic flow v_2 and the nuclear modification factor R_{AA}.

DOI: 10.1103/PhysRevC.93.014901

I. INTRODUCTION

One major goal of ultrahigh-energy heavy ion physics is to recreate the phase of deconfined quarks and gluons (quark gluon plasma; QGP) as it might have existed a few microseconds after the Big Bang. Various experimental facilities have been built to explore the properties of this QGP experimentally, while on the theory side a multitude of (potential) signatures and properties of the QGP have been predicted [1–3].

Heavy quarks are an ideal probe for QGP. They are produced at the beginning of the collision in hard processes and therefore probe the created medium during its entire evolution. When the system cools down they hadronize, and their decay products can finally be detected. By investigating heavy quark observables we can thus explore the interaction processes within a hot and dense medium. Two of the most interesting observables are the nuclear modification factor, R_{AA}, and the elliptic flow, v_2. Experimentally, the nuclear modification factor shows a large suppression of the open heavy flavor particles' spectra at high transverse momenta (p_T) compared to the findings in pp collisions. This indicates a high degree of thermalization also of heavy quarks with a bulk medium consisting of light quarks and gluons and, perhaps at later stages of fireball evolution, hot and dense hadron gas. The measured large elliptic flow, v_2, of open heavy flavor mesons and nonphotonic single electrons or muons from their semileptonic decay supports this interpretation because it indicates that heavy quarks take part in the collective motion of the bulk medium. A quantitative analysis of the degree of thermalization of heavy quark degrees of freedom in terms of the microscopic scattering processes may lead to an understanding of the mechanisms underlying the high coupling strength of the QGP and the corresponding transport properties.

In this paper we explore the medium modification of heavy flavor p_T spectra, using a hybrid model, consisting of the ultrarelativistic quantum molecular dynamics (UrQMD) model [4,5] and a full (3+1)-dimensional ideal hydrodynamical model [6,7] to simulate the bulk medium. Heavy quark propagation in the medium is described by a relativistic Langevin approach [8]. Similar studies have recently been performed in a thermal fireball model with a combined coalescence-fragmentation approach [8–14], in an ideal hydrodynamics model with a lattice-QCD equation of state (EoS) [15,16], in a model by Kolb and Heinz [17], in the BAMPS model [18,19], and in the MARTINI model [20] as well as in further studies and model comparisons [21–25].

The use of hybrid models (such as the UrQMD hybrid model used here) provides a major step forward compared to simplified parametrizations of the temperature and flow. It provides a realistic and well-established background, particularly initial conditions for the hydrodynamical evolution of the medium. Additionally, it also includes event-by-event fluctuations and has been shown to describe well many collective properties of relativistic heavy ion collisions. For heavy quark propagation we apply a Langevin approach during the hydrodynamical evolution of the hot and dense medium, employing drag and diffusion coefficients from two effective

*inghirami@fias.uni-frankfurt.de

models for elastic scattering between heavy quarks and light quarks and gluons based on (a) an effective heavy quark model and the formation of D- or B-meson-like resonances in the QGP [26,27] or (b) a Dirac-Brueckner T-matrix evaluation of the corresponding cross sections based on static heavy quark potentials from lattice QCD [9]. The hadronization of heavy quarks to D or B mesons is described using a fragmentation or coalescence approach. Within this framework we investigate the effects of using different drag and diffusion coefficients, different freeze-out temperatures of heavy flavors on the heavy quark observables, and different hadronization descriptions and compare the results with experimental data from the Relativistic Heavy Ion Collider (RHIC) and the Large Hadron Collider (LHC).

II. THE UrQMD HYBRID MODEL

To extract information on the interaction of heavy quarks with the medium one ideally applies a well-tested model for the (collective) dynamics of bulk matter. In heavy ion collisions the medium is by no means homogeneous. Rather it is a rapidly expanding system fluctuating locally and event by event. In our calculation we employ the state-of-the-art UrQMD hybrid model for the description of the expanding background. This model has been developed in recent years to combine the advantages of hadronic transport theory and ideal fluid dynamics [28]. To account for the nonequilibrium dynamics in the very early stage of the collision in the hybrid model, the UrQMD cascade [4,5] is used to calculate the initial states of the heavy ion collisions, each to be used in a subsequent hydrodynamical evolution [29]. In the present study, the transition from the UrQMD initial state to the hydrodynamical evolution takes place at a time $t = 0.5$ fm, which, for RHIC and LHC energies, can be considered an appropriate value to reproduce the bulk properties of the fluid as measured in experiments [30] within hydrodynamical models. The energy, baryon number, and momentum of all particles within UrQMD are mapped onto a spatial grid for the hydrodynamic evolution including event-by-event fluctuations. The full (3+1)-dimensional ideal hydrodynamic evolution is performed using the SHASTA algorithm [6,7]. We solve the equations for the conservation of energy and momentum and for the conservation of the baryonic charge. With $T^{\mu\nu}$ denoting the relativistic energy-momentum tensor the corresponding equations read

$$\partial_\mu T^{\mu\nu} = 0, \tag{1}$$

and for the baryon four-current N^μ

$$\partial_\mu N^\mu = 0. \tag{2}$$

To transfer all particles back into the UrQMD model, an approximate iso-proper-time transition is chosen (see [31] for details). Here, we apply the Cooper-Frye prescription [32] and transform to particle degrees of freedom via

$$E\frac{\mathrm{d}N}{d^3p} = g_i \int_\sigma \mathrm{d}\sigma_\mu p^\mu f(x,p). \tag{3}$$

Here $\mathrm{d}\sigma_\mu = (\mathrm{d}^3x, 0,0,0))$ is the hypersurface normal. In Eq. (3) $f(x,p)$ are the Bose- and Fermi-distribution functions, and g_i the degeneracy factors for the different particle species. After "particlization" evolution proceeds in the hadronic cascade (UrQMD), where final rescatterings and decays are calculated until all interactions cease and the system decouples. However, since below the decoupling temperature we let the D and B mesons propagate without further hadronic interactions, this final part of the evolution does not affect the v_2 and R_{AA} observables. A more detailed description of the hybrid model including parameter tests and results is given in [28]. A comparison to the results employing a nonapproximated hypersurface is given in [33].

III. HEAVY QUARK DIFFUSION

The diffusion of a "heavy particle" in a medium consisting of "light particles" can be described with a Fokker-Planck equation [9,21,26,27,34–36]. Here one approximates the collision term of the corresponding Boltzmann equation, which in turn can be mapped into an equivalent stochastic Langevin equation.

A. Relativistic Langevin approach

In the relativistic realm such a Langevin process reads

$$\begin{aligned} \mathrm{d}x_j &= \frac{p_j}{E}\mathrm{d}t, \\ \mathrm{d}p_j &= -\Gamma p_j \mathrm{d}t + \sqrt{\mathrm{d}t}\, C_{jk}\rho_k. \end{aligned} \tag{4}$$

Here $\mathrm{d}t$ is the time step in the Langevin calculation, $\mathrm{d}x_j$ and $\mathrm{d}p_j$ are the coordinate and momentum changes in each time step, $E = \sqrt{m^2 + \boldsymbol{p}^2}$, and Γ is the drag or friction coefficient. The covariance matrix, C_{jk}, of the fluctuating force is related to the diffusion coefficients, as we see below. Both Γ and C_{jk} depend on $(t,\boldsymbol{x},\boldsymbol{p})$ and are defined in the (local) rest frame of the fluid. The ρ_k are Gaussian-normal-distributed random variables. Their distribution function reads

$$P(\boldsymbol{\rho}) = \left(\frac{1}{2\pi}\right)^{3/2} \exp\left(-\frac{\boldsymbol{\rho}^2}{2}\right), \tag{5}$$

with $\boldsymbol{\rho} = (\rho_1,\rho_2,\rho_3)$. The fluctuating force $F_j^{(\mathrm{fl})}$ thus obeys

$$\left\langle F_j^{(\mathrm{fl})}(t)\right\rangle = 0, \quad \left\langle F_j^{(\mathrm{fl})}(t)F_k^{(\mathrm{fl})}(t')\right\rangle = C_{jl}C_{kl}\delta(t-t'). \tag{6}$$

It is important to note that with these specifications the random process is not yet uniquely determined since one has to specify at which momentum argument the covariance matrix C_{jk} has to be taken to define the stochastic time integral in (4). As we derive now, the demand that the Brownian particle reach the correct equilibrium-phase-space distribution in the long-time limit of the stochastic process leads to dissipation-fluctuation relations between the drag and the diffusion coefficients [37]. Another approach is to derive the Fokker-Planck equation that is equivalent to the Langevin process as an approximation of the collision term in the Boltzmann equation and adjust the drag coefficient and the covariance matrix accordingly [38]. In the following we derive the Fokker-Planck equation for the heavy quark phase-space distribution function from the Langevin process defined, (4)–(6), and use the constraint by the correct long-time equilibrium limit to establish the dissipation-fluctuation relations between the drag and the diffusion coefficients for different realizations of the Langevin process.

These realizations are defined by the choice of the stochastic integral implied by the contribution of the stochastic force in the momentum-update rule in (4) via a parameter $\xi \in [0,1]$, determining the momentum argument in the covariance matrix of the white noise [cf. (6)]:

$$C_{jk} = C_{jk}(t,\boldsymbol{x},\boldsymbol{p}+\xi \mathrm{d}\boldsymbol{p}). \tag{7}$$

For $\xi = 0$, $\xi = 1/2$, and $\xi = 1$ the corresponding Langevin processes are called the prepoint Ito, the midpoint Stratonovich-Fisk, and the postpoint Ito (or Hänggi-Klimontovich) realization, respectively [39].

To derive the Fokker-Planck equation for any choice of $\xi \in [0,1]$ we consider the time evolution of the average of an arbitrary phase-space function $g(\boldsymbol{x},\boldsymbol{p})$. To this end we use (4) and (6) with the momentum argument of C_{jk} defined in (7) to derive the time derivative of this expectation value along the stochastic trajectory of the Brownian particle. To this end we need a Taylor expansion with respect to $\mathrm{d}\boldsymbol{x}$ and $\mathrm{d}\boldsymbol{p}$ up to second order, because the time step is of order $\mathcal{O}(\sqrt{\mathrm{d}t})$ due to the stochastic force:

$$\begin{aligned}\mathrm{d}g &= g(\boldsymbol{x}+\mathrm{d}\boldsymbol{x},\boldsymbol{p}+\mathrm{d}\boldsymbol{p}) - g(\boldsymbol{x},\boldsymbol{p})\\ &= \frac{\partial g}{\partial x_j}\mathrm{d}x_j + \frac{\partial g}{\partial p_j}\mathrm{d}p_j + \frac{1}{2}\frac{\partial^2 g}{\partial p_j \partial p_k}\mathrm{d}p_j\mathrm{d}p_k + \mathcal{O}(\mathrm{d}t^{3/2}).\end{aligned} \tag{8}$$

Here and in the following we use the Einstein-summation convention; i.e., we sum over repeated indices. Now we have to take the ensemble average of this equation. We consider the three terms on the right-hand side separately, using (4)–(7):

$$\left\langle \frac{\partial g}{\partial x_j}\mathrm{d}x_j \right\rangle = \left\langle \frac{\partial g}{\partial x_j}\frac{p_j}{E}\mathrm{d}t \right\rangle = \frac{\partial g}{\partial x_j}\frac{p_j}{E}\mathrm{d}t, \tag{9}$$

$$\begin{aligned}\left\langle \frac{\partial g}{\partial p_j}\mathrm{d}p_j \right\rangle &= \left\langle \frac{\partial g}{\partial p_j}[-\Gamma p_j \mathrm{d}t + C_{jk}(\boldsymbol{p}+\xi\mathrm{d}\boldsymbol{p})\rho_k\sqrt{\mathrm{d}t}] \right\rangle\\ &= \left\langle \frac{\partial g}{\partial p_j}\left[-\Gamma p_j \mathrm{d}t + \left(C_{jk}(\boldsymbol{p})\rho_k + \frac{\partial C_{jk}(\boldsymbol{p})}{\partial p_l} \right.\right.\right.\\ &\qquad \left.\left.\left. \times \xi C_{lm}(\boldsymbol{p})\rho_k\rho_m\sqrt{\mathrm{d}t}\right)\sqrt{\mathrm{d}t}\right]\right\rangle + \mathcal{O}(\mathrm{d}t^{3/2})\\ &= \frac{\partial g}{\partial p_j}\left[-\Gamma p_j + \xi\frac{\partial C_{jk}(\boldsymbol{p})}{\partial p_l}C_{lk}(\boldsymbol{p})\right]\mathrm{d}t + \mathcal{O}(\mathrm{d}t^{3/2})\end{aligned} \tag{10}$$

$$\left\langle \frac{1}{2}\frac{\partial^2 g}{\partial p_j \partial p_k}\mathrm{d}p_j\mathrm{d}p_k \right\rangle = \frac{1}{2}\frac{\partial^2 g}{\partial p_j \partial p_k}C_{jl}(\boldsymbol{p})C_{kl}(\boldsymbol{p})\mathrm{d}t + \mathcal{O}(\mathrm{d}t^{3/2}). \tag{11}$$

Combining (9)–(11), we finally obtain

$$\begin{aligned}&\langle g(\boldsymbol{x}+\mathrm{d}\boldsymbol{x},\boldsymbol{p}+\mathrm{d}\boldsymbol{p}) - g(\boldsymbol{x},\boldsymbol{p})\rangle\\ &= \left[\frac{\partial g}{\partial x_j}\frac{p_j}{E} + \frac{\partial g}{\partial p_j}\left(-\Gamma p_j + \xi\frac{\partial C_{jk}}{\partial p_l}C_{lk}\right)\right.\\ &\quad \left. + \frac{1}{2}\frac{\partial^2 g}{\partial p_j \partial p_k}C_{jl}C_{kl}\right]\mathrm{d}t + \mathcal{O}(\mathrm{d}t^{3/2}).\end{aligned} \tag{12}$$

Here all momentum arguments of the drag and diffusion coefficients have to be taken at the argument $\boldsymbol{p}$. From (12) via

$$\begin{aligned}\langle g(\boldsymbol{x},\boldsymbol{p})\rangle &= \int_{\mathbb{R}^3}\mathrm{d}^3\boldsymbol{x}\int_{\mathbb{R}^3}\mathrm{d}^3\boldsymbol{p}\, f(t,\boldsymbol{x},\boldsymbol{p})g(\boldsymbol{x},\boldsymbol{p}),\\ \left\langle \frac{\mathrm{d}}{\mathrm{d}t}g(\boldsymbol{x},\boldsymbol{p})\right\rangle &= \int_{\mathbb{R}^3}\mathrm{d}^3\boldsymbol{x}\int_{\mathbb{R}^3}\mathrm{d}^3\boldsymbol{p}\;\partial_t f(t,\boldsymbol{x},\boldsymbol{p})g(\boldsymbol{x},\boldsymbol{p})\\ &\overset{(12)}{=} \int_{\mathbb{R}^3}\mathrm{d}^3\boldsymbol{x}\int_{\mathbb{R}^3}\mathrm{d}^3\boldsymbol{p}\; f(t,\boldsymbol{x},\boldsymbol{p})\\ &\quad \times\left[\frac{\partial g}{\partial x_j}\frac{p_j}{E} + \frac{\partial g}{\partial p_j}\left(-\Gamma p_j + \xi\frac{\partial C_{jk}}{\partial p_l}C_{lk}\right)\right.\\ &\quad \left. + \frac{1}{2}\frac{\partial^2 g}{\partial p_j \partial p_k}C_{jl}C_{kl}\right]\end{aligned} \tag{13}$$

and integrating by part in the final expression, it follows immediately that the time evolution of the phase-space distribution function $f_Q(t,\boldsymbol{x},\boldsymbol{p})$ of heavy quarks is given by the Fokker-Planck equation,

$$\frac{\partial f_Q}{\partial t} + \frac{p_j}{E}\frac{\partial f_Q}{\partial x_j} = \frac{\partial}{\partial p_j}(Ap_j f_Q) + \frac{\partial^2}{\partial p_j \partial p_k}(B_{jl} f_Q), \tag{14}$$

where the coefficients Ap_j and diffusion coefficients

$$\begin{aligned}B_{jk} &= B_{kj} = B_0 P^{\perp}_{jk} + B_1 P^{\parallel}_{jk},\\ \text{with}\quad P^{\parallel}_{jk} &= \frac{p_j p_k}{\boldsymbol{p}^2},\quad P^{\perp}_{jk} = \delta_{jk} - \frac{p_j p_k}{\boldsymbol{p}^2},\end{aligned} \tag{15}$$

for an isotropic medium are related to the pertinent parameters in the Langevin process by

$$Ap_j = \Gamma p_j - \xi C_{lk}\frac{\partial C_{jk}}{\partial p_l}, \tag{16}$$

$$C_{jk} = \sqrt{2B_0}P^{\perp}_{jk} + \sqrt{2B_1}P^{\parallel}_{jk}. \tag{17}$$

In the case of a background medium at thermal equilibrium (a "heat bath"),[1] the stationary limit should become a Boltzmann-Jüttner distribution with the temperature of the heat bath. Thus, one typically adjusts the drag coefficient by choosing the longitudinal diffusion coefficient, B_1, in (17) so as to satisfy this asymptotic equilibration condition [38], leading to dissipation-fluctuation relations between this diffusion coefficient and the drag coefficient [8,21].

It turns out that for $B_0 = B_1 = D(E)$ and a homogeneous background medium the Boltzmann-Jüttner distribution,

$$f^{(\mathrm{eq})}_Q(\boldsymbol{p}) = \exp\left(-\frac{E}{T}\right),\quad \text{with } E = \sqrt{\boldsymbol{p}^2 + m^2}, \tag{18}$$

becomes a solution of the corresponding stationary Fokker-Planck equation, if the dissipation-fluctuation relation

$$\Gamma(E)ET - D(E) + T(1-\xi)D'(E) = 0 \tag{19}$$

[1] In numerical studies it has turned out that drag and diffusion coefficients as obtained from microscopic models usually do not lead to the expected long-time stationary limit of the phase-space distribution for heavy particles when diffusing in an equilibrated background medium.

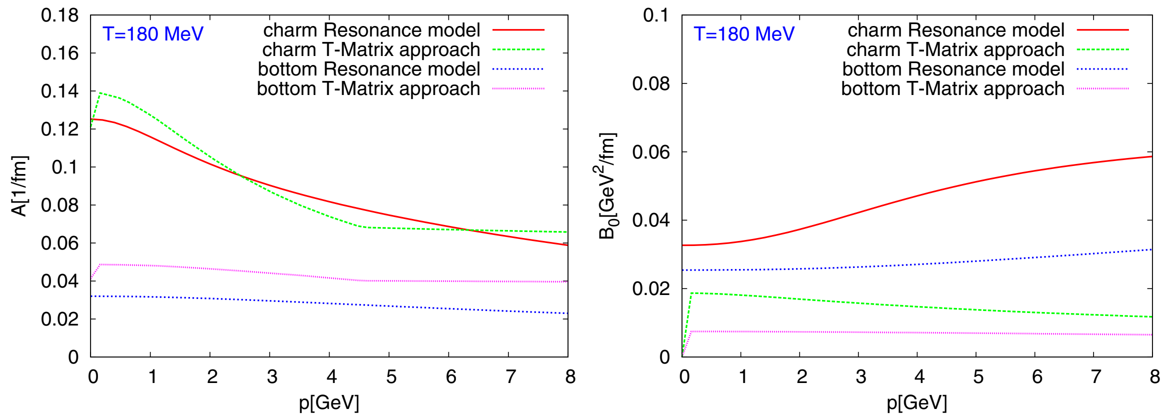

FIG. 1. Drag (left) and diffusion (right) coefficients in the resonance model and the T-matrix approach for charm and bottom quarks. The plot shows the dependence of the coefficients on the three-momentum $|\vec{p}|$ at a fixed temperature $T = 180$ MeV.

is fulfilled. A straightforward way to achieve the correct asymptotic equilibrium distribution within a relativistic Langevin simulation is to set $\xi = 1$ (i.e., using the postpoint Ito realization), which reduces (19) to

$$D(E) = \Gamma(E)ET. \tag{20}$$

For applications to heavy ion collisions we use Γ from underlying microscopic models for heavy quark scattering with light quarks and gluons as detailed below and adjust the diffusion coefficients B_0 (transverse) and B_1 (longitudinal) to

$$B_0 = B_1 = \Gamma ET. \tag{21}$$

So far we have defined our Langevin process with respect to the (local) rest frame of the background medium. For a medium with collective flow, one has to evaluate the time step in the local rest frame and boost back to the computational frame. For a closer look at the postpoint description see Sec. A 1.

For heavy quark propagation in the Langevin model we also need transport coefficients. In this work these drag and diffusion coefficients are obtained from two nonperturbative models for elastic heavy quark scattering, a resonance model, where the existence of D mesons and B mesons in the QGP phase is assumed, as well as a T-matrix approach, in which quark-antiquark potentials are used for calculation of the coefficients in the QGP. They are described in detail in Sec. A 2 and are shown in Fig. 1 as a function of the three-momentum $|\vec{p}|$ at $T = 180$ MeV and in Fig. 2 as a function of the temperature at a fixed three-momentum of $|\vec{p}| = 0.8$ GeV. In the Appendix A 3 we compare the two sets of coefficients used in this article with a third one kindly provided by the Nantes group, based on a hard-thermal-loop model.

B. Implementation of the Langevin simulation in the UrQMD-hybrid model

For the present study, charm production and propagation are evaluated perturbatively in the time-dependent background generated by the UrQMD/hybrid model. To model a fluctuating and space-time-dependent Glauber initial-state geometry, we perform the first UrQMD run with elastic 0° scatterings between the colliding nuclei and save the nucleon-nucleon collision space-time coordinates. These coordinates are used in the second, full UrQMD run as (possible) production coordinates for heavy quarks.

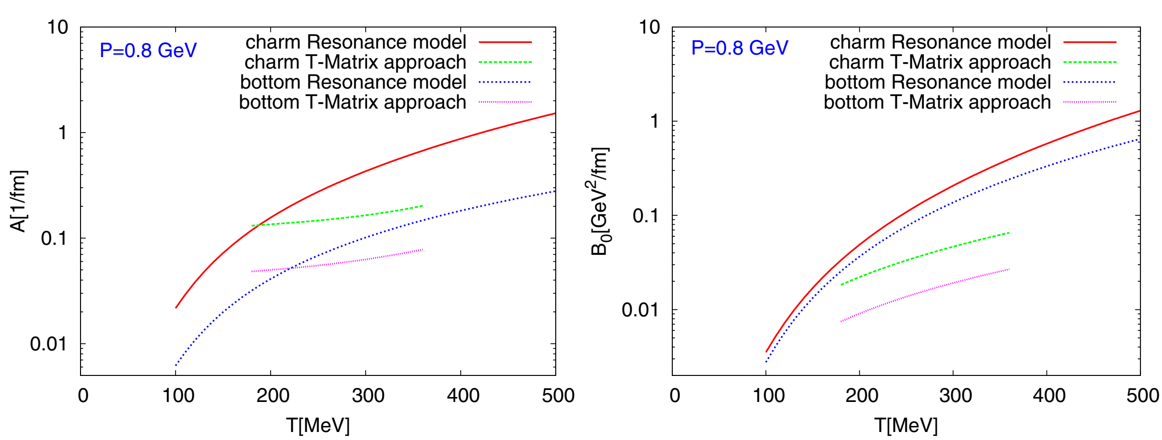

FIG. 2. Drag (left) and diffusion (right) coefficients in the resonance model and the T-matrix approach for charm and bottom quarks. The plot shows the dependence of the coefficients on the temperature at a fixed three-momentum $|\vec{p}| = 0.8$ GeV. The T-matrix coefficients are calculated between 180 and 360 MeV only.

As the momentum distribution for the initially produced charm quarks at $\sqrt{s_{NN}} = 200$ GeV we use

$$\frac{1}{2\pi p_T dp_T} = \frac{(A_1 + p_T)^2}{(1 + A_2 \cdot p_T)^{A_3}}, \tag{22}$$

with $A_1 = 0.5$, $A_2 = 0.1471$, and $A_3 = 21$, and for bottom quarks

$$\frac{1}{2\pi p_T dp_T} = \frac{1}{\left(A_1 + p_T^2\right)^{A_2}}, \tag{23}$$

with $A_1 = 57.74$ and $A_2 = 5.04$. These distributions are taken from [9] and [27] and are shown in Fig. 3. They are obtained by using tuned c-quark spectra from PYTHIA. Their pertinent semileptonic single-electron decay spectra account for pp and dAu measurements by STAR up to 4 GeV. The missing part at higher p_T is then supplemented by B-meson contributions.

Starting with these charm and bottom quark distributions as initial conditions we perform, as soon as the hydrodynamics start condition is fulfilled, an Ito postpoint time step of our Langevin simulation, as described in Sec. III A, at each time step of the hydrodynamical evolution. We use the cell velocities, cell temperatures, length of the time step, and γ factor of the cells to calculate the momentum transfer, propagating all heavy quarks independently. For the Langevin transport we use the drag and diffusion coefficients obtained from the resonance model or T-matrix approach as described in Sec. A 2.

To analyze the sensitivity of R_{AA} and, especially, v_2 to the decoupling time of the heavy flavors from the medium we vary the decoupling temperatures between 130 and 180 MeV (for the resonance model) and extrapolate the corresponding transport coefficients smoothly into the hadronic phase. This assumption of a smooth transition of the transport coefficients in the transition from the partonic description above and the hadronic one below T_c has been verified, using an effective model for open heavy flavor interactions in a hadronic medium in [15] and [41].

Our approach provides us with the heavy quark momentum distribution. We include a hadronization mechanism for open heavy flavor mesons (D and B mesons). Since nonphotonic single electrons are usually measured in experiments, we perform a semileptonic decay into electrons as the final step to compare to data. In addition, we provide D- and B-meson results for direct comparisons to the upcoming direct D/B measurements by the STAR Heavy Flavor Tracker. These results are reported in Sec. A 4.

IV. RESULTS AT RHIC ENERGIES

A. Elliptic flow v_2 and nuclear modification factor R_{AA} with fragmentation

Figure 4 presents the elliptic flow, v_2, of charm and bottom quarks from Au + Au collisions at $\sqrt{s_{NN}} = 200$ GeV in the centrality range $\sigma/\sigma_{\text{tot}} = 20\%$–$40\%$ applying a rapidity cutoff of $|y| < 0.35$. For our calculation using the drag and diffusion coefficients of the T-matrix model we use a decoupling temperature of 180 MeV, while with the resonance model we show results for decoupling temperatures of 130, 150, and 180 MeV.

As one can clearly see, the elliptic flow, v_2, of bottom quarks (thin lines) is much smaller compared to that of charm quarks (thick lines) due to their larger mass. Furthermore, use of the coefficients from the T-matrix model compared with those from the resonance model shows that both calculations are in reasonable agreement. The elliptic flow of the charm quarks is, nevertheless, somewhat lower for the T-matrix model than for the resonance model. With decreasing decoupling temperature the flow clearly increases. Thus, we conclude that the late phase of the heavy ion collision may have considerable influence on the heavy flavor elliptic flow, although the drag and diffusion coefficients become small in the late stages of fireball evolution.

Moreover, the v_2 is shifted towards higher p_T for lower decoupling temperatures. This effect is due to the increased radial velocity of the medium, which, in the case of a developed elliptic flow, is larger in the x than in the y direction. Consequently there is a depletion of particles with high v_x in the low-p_T region and smaller elliptic flow. This effect is more important for heavier particles and a larger radial flow [42,43].

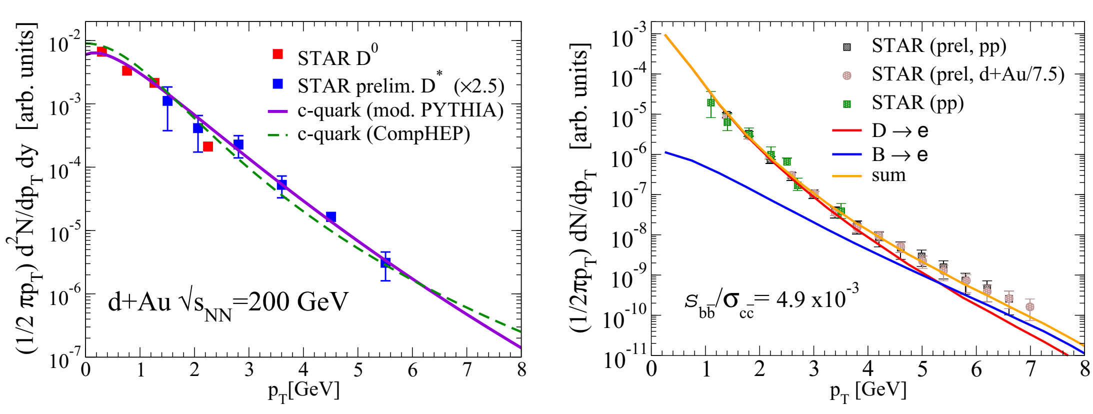

FIG. 3. Fits of D- and D*-meson p_T spectra in 200 A GeV d-Au collisions at the RHIC with a modified PYTHIA simulation (left) and the corresponding nonphotonic single-electron p_T spectra in pp and d-Au collisions (taken from [40]) (right). The missing yield of high-p_T electrons is fitted with the analogous B-meson decay spectra, thus fixing the bottom-to-charm ratio at $\sigma_{b\bar{b}}/\sigma_{c\bar{c}} \simeq 4.9 \times 10^{-3}$.

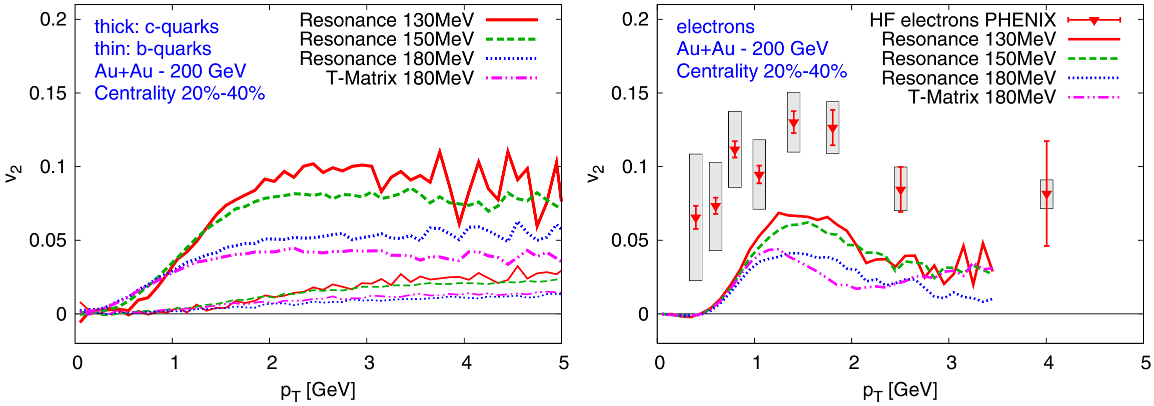

FIG. 4. Left: Elliptic flow, v_2, of heavy quarks in Au + Au collisions at $\sqrt{s_{NN}} = 200$ GeV. We use a rapidity cutoff of $|y| < 0.35$. Thick lines depict charm quarks, while thin lines depict bottom quarks. Right: Elliptic flow, v_2, of electrons from heavy meson decays using Peterson fragmentation to D/B mesons and subsequent decay into electrons in Au + Au collisions at $\sqrt{s_{NN}} = 200$ GeV. We use a rapidity cutoff of $|y| < 0.35$. Data are from [48].

To compare our calculations with data on nonphotonic electrons from the RHIC we perform (in the computational frame) a Peterson fragmentation of the charm and bottom quarks to D mesons and B mesons using the fragmentation function from [44]

$$D_Q^H(z) = \frac{N}{z[1 - (1/z) - \epsilon_Q/(1 - z)]^2},$$

where N is a normalization constant, z the relative-momentum fraction obtained in the fragmentation of the heavy quark, and $\epsilon_Q = 0.05$ (0.005) for charm (bottom) quarks [45]. After hadronization we use PYTHIA routines for the semileptonic decay to electrons [46,47].

Figure 4 shows our results for v_2 for single electrons in comparison to data from the PHENIX Collaboration.

Again, we clearly observe the importance of the late phase of the collision. The depletion effect at low p_T described before is clearly visible. The decrease in the elliptic flow at high p_T is due to the increasing fraction of electrons from bottom decays, which have a lower v_2 as shown in Fig. 4. The calculated flow in the setup with Peterson fragmentation is too small compared to the PHENIX data.

The corresponding nuclear modification factor, R_{AA}, for heavy quarks is shown in Fig. 5. Again, we present results for Au + Au collisions at $\sqrt{s_{NN}} = 200$ GeV in the centrality range 20%–40%. The quenching for charm quarks is, as expected, much stronger than that for bottom quarks. While for bottom quarks the suppression at high p_T is moderate, R_{AA} may drop to 20%–30% for charm quarks. The influence of the medium is, as already seen in our flow calculations, larger for a lower decoupling temperature, underlining the importance of the late stage of the collision. Figure 5 shows the comparison of our non-photonic-electron R_{AA} to the data taken by the PHENIX Collaboration.

The nuclear modification factor drops quite rapidly and stabilizes at about $p_T \gtrsim 2$ GeV. Around $p_T \approx 2$ GeV it is significantly below the PHENIX data. For higher p_T the calculated R_{AA} approaches the measured data, especially for low decoupling temperatures. This effect is due to the increasing flow of the heavy flavor particles with decreasing

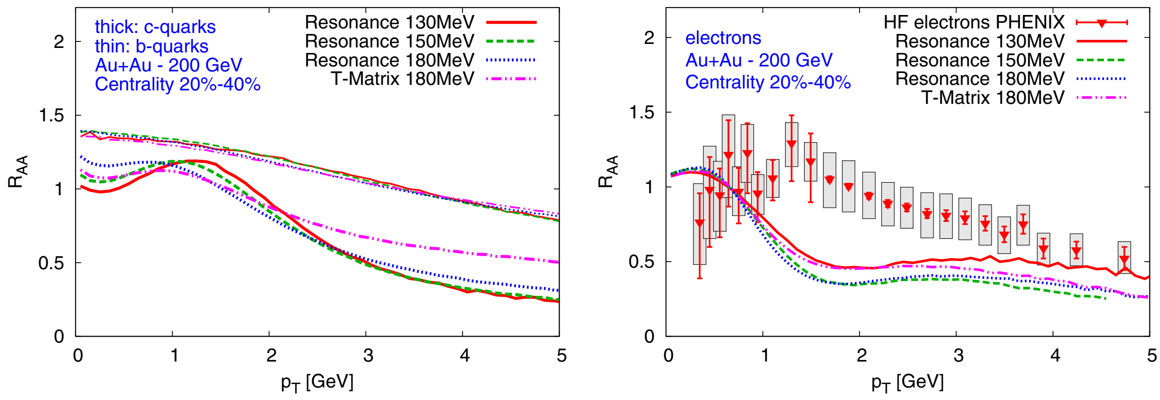

FIG. 5. Left: R_{AA} of heavy quarks in Au + Au collisions at $\sqrt{s_{NN}} = 200$ GeV. We use a rapidity cutoff of $|y| < 0.35$. Thick lines depict charm quarks, while thin lines depict bottom quarks. Right: R_{AA} of electrons from heavy quark decays in Au + Au collisions at $\sqrt{s_{NN}} = 200$ GeV compared to RHIC data [48]. We use a rapidity cutoff of $|y| < 0.35$. The high-p_T suppression turns out to be too strong compared with the data.

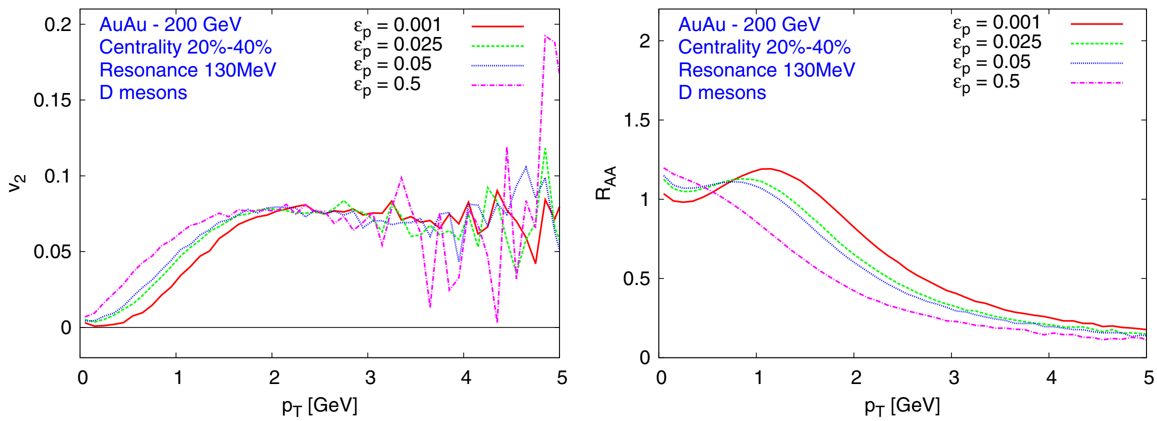

FIG. 6. Elliptic flow v_2 (left) and R_{AA} (right) of D mesons using different ϵ_Q values in the Peterson fragmentation function.

decoupling temperature, which pushes low-p_T heavy flavor particles towards higher-p_T bins.

B. Effect of different ϵ_Q values in the Peterson fragmentation function

To explore the influence of different ϵ_Q values in the Peterson fragmentation function, see Fig. 6. The calculations are performed for the resonance model without a modification factor, i.e., with $k = 1$.

One observes that modification of the epsilon parameter has some influence on the final observables. However, even in this wide range of parameters one is not able to find a parameter that allows an explanation of both the elliptic flow data and the nuclear modification factor. The problem is that for $\epsilon_Q \to 0$ the edge of the $v_2(p_T)$ and the peak in R_{AA} move to higher p_T values. While the data support a shift of the R_{AA} peak towards higher p_T values (i.e., lower ϵ_Q values), an improved description of the elliptic flow would benefit from a shift of the edge of the $v_2(p_T)$ towards a lower p_T.

C. Elliptic flow v_2 and nuclear modification factor R_{AA} using a k factor

In the previous section we learned that the elliptic flow of heavy quarks in the calculation with fragmentation is too small compared to the experimental data. One possibility to improve this problem is to multiply the drag and diffusion coefficients with a "k factor." Therefore we have performed the same calculations as in the last section but using a k factor of 3.

As shown in Fig. 7 the elliptic flow increases considerably due to the stronger coupling of heavy quarks to the hot medium. The results after performing the Peterson fragmentation and the subsequent decays to electrons are shown in Fig. 7. The elliptic flow is now comparable to the data, especially when using the low decoupling temperature of 130 MeV. Only at low p_T do we underestimate the flow due to the depletion effect described above.

Our results for the nuclear modification factor, R_{AA}, are depicted in Fig. 8. The quenching is much stronger than for the calculation without a k factor. Figure 8 shows the results

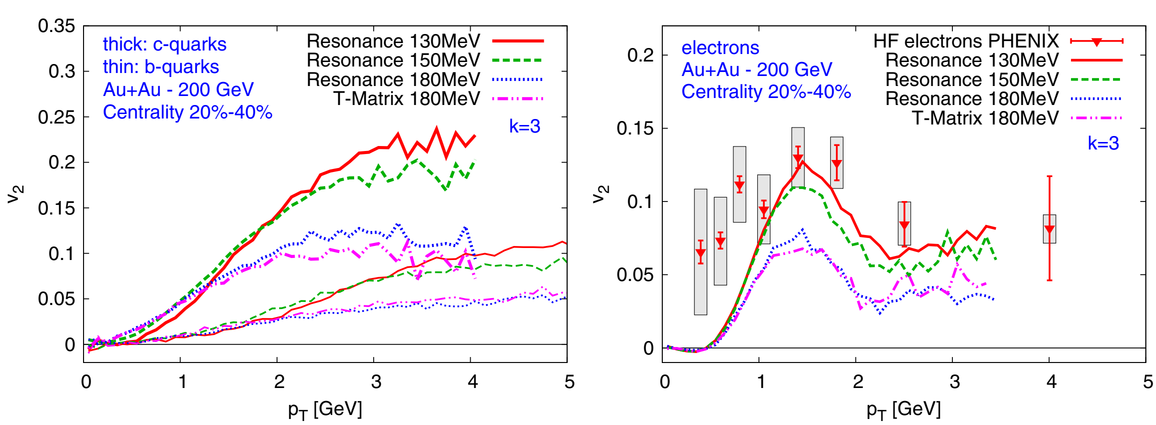

FIG. 7. Left: Elliptic flow, v_2, of heavy quarks in Au + Au collisions at $\sqrt{s_{NN}} = 200$ GeV employing a k factor of 3. We use a rapidity cutoff of $|y| < 0.35$. Thick lines depict charm quarks, while thin lines depict bottom quarks. Right: Elliptic flow, v_2, of electrons from heavy quark decays in Au + Au collisions at $\sqrt{s_{NN}} = 200$ GeV employing a k factor of 3. We use a rapidity cutoff of $|y| < 0.35$. The flow in our calculation using a k factor is comparable to the data [48].

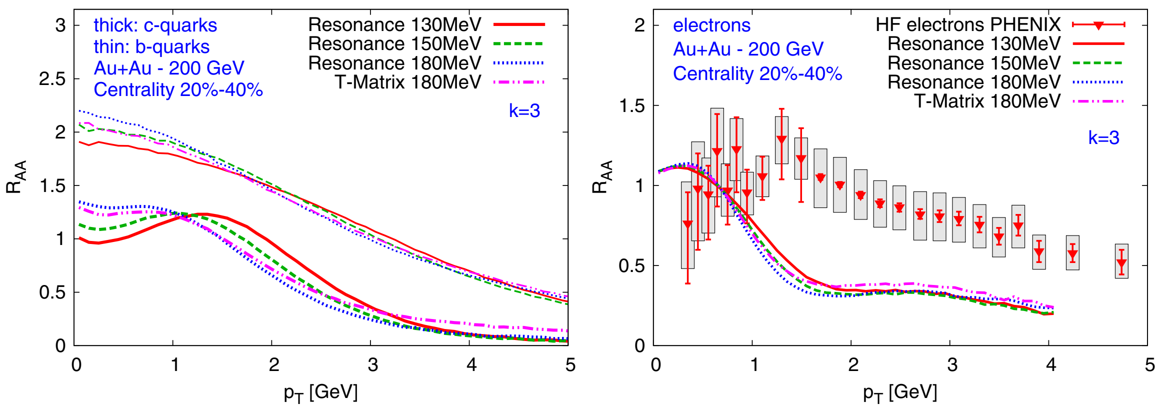

FIG. 8. Left: R_{AA} of electrons from heavy flavor decays in Au + Au collisions at $\sqrt{s_{NN}} = 200$ GeV employing a k factor of 3. We use a rapidity cutoff of $|y| < 0.35$. Thick lines show the results for charm quarks, and thin lines for bottom quarks. Right: v_2 of electrons from heavy flavor decays in Au + Au collisions at $\sqrt{s_{NN}} = 200$ GeV employing a k factor of 3. We use a rapidity cutoff of $|y| < 0.35$. As expected the medium modification is stronger than without a k factor. Data are taken from [48].

for electrons. The suppression of nonphotonic electrons at high p_T is also stronger than for the calculation without a k factor.

We conclude that the use of a k factor can improve the description of the elliptic flow. However, it is not possible to reach a consistent simultaneous description of both the elliptic flow and the nuclear modification factor using the same k factor.

D. Elliptic flow v_2 and nuclear modification factor R_{AA} using coalescence

Instead of describing heavy quark hadronization by Peterson fragmentation (and/or an additional k factor, as discussed above), one can alternatively apply a quark coalescence approach for D- and B-meson production. To implement this coalescence we perform the Langevin calculation until the decoupling temperature is reached. Subsequently we coalesce a light quark with a heavy quark. As the light quarks constitute the medium propagated by hydrodynamics, the average velocities of the light quarks can be (on average) approximated by the flow velocities of the hydro cells. The mass of the light quarks is assumed to be 370 MeV so that the D-meson mass becomes 1.87 GeV when the masses of the light quarks and the charm quarks (1.5 GeV) are added. Since we assume the light quarks to have the same mass when coalescing with bottom quarks (4.5 GeV), the B mesons obtain a mass of 4.87 GeV.

The differences in the flow and the spectra of D and B mesons when comparing Peterson fragmentation (without k-factor) to the coalescence model is shown in Fig. 9. These calculations are performed employing a decoupling temperature of 150 MeV.

Compared to the fragmentation case, the elliptic flow reaches higher values at high p_T due to the coalescence. Also, the depletion effect described before is more pronounced. Regarding the nuclear modification factor, the difference between Peterson fragmentation and the coalescence model is even larger. The push of low-p_T particles to higher p_T values is stronger in the case of the coalescence model, while the suppression of heavy mesons at high p_T values is stronger in the case of Peterson fragmentation.

Again, we perform a decay to electrons using PYTHIA for comparison to experimental measurements from the PHENIX Collaboration. Figure 10 (left) shows our results for v_2. Due to the coalescence the elliptic flow is strongly increased

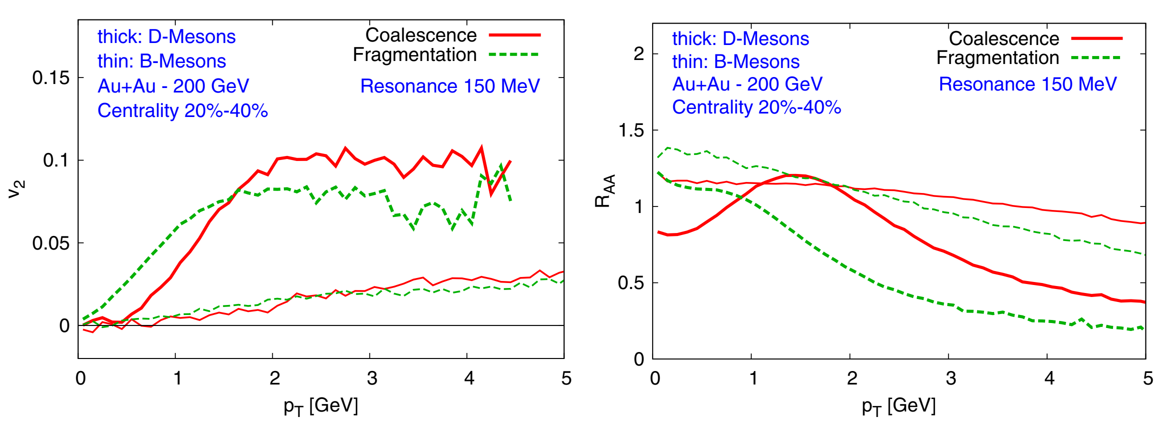

FIG. 9. Elliptic flow v_2 (left) and R_{AA} (right) of D mesons (thick lines) and B mesons (thin lines) in Au + Au collisions at $\sqrt{s_{NN}} = 200$ GeV. We use a rapidity cutoff of $|y| < 0.35$. A comparison of Peterson fragmentation and coalescence with light quarks is shown. For the drag and diffusion coefficients we use the resonance model with a decoupling temperature of 150 MeV.

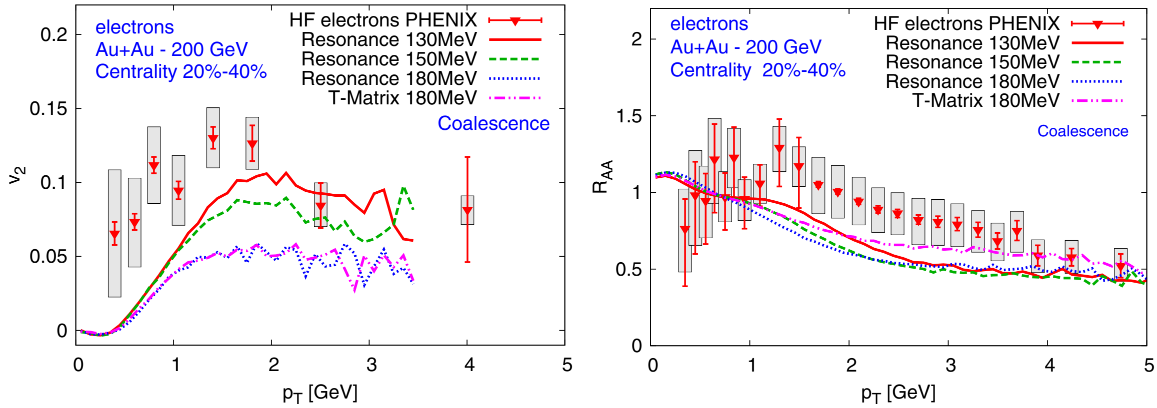

FIG. 10. Elliptic flow v_2 (left) and nuclear modification factor R_{AA} (right) of electrons from heavy quark decays in Au + Au collisions at $\sqrt{s_{NN}} = 200$ GeV using a coalescence mechanism. We use a rapidity cutoff of $|y| < 0.35$. For a decoupling temperature of 130 MeV we find a reasonable agreement with the data [48].

compared to the previous calculation using the Peterson fragmentation. This higher flow is due to the momentum kick of light quarks in the recombination process, which provides additional flow from the medium. For a decoupling temperature of 130 MeV we obtain a reasonable agreement with the experimental data.

In Fig. 10 (right) the nuclear modification factor for nonphotonic single electrons is depicted.

Also here we obtain a good agreement with the data. Especially at a moderate $p_T \simeq 2$ GeV, the calculation has strongly improved. The coalescence mechanism pushes the heavy quarks to higher p_T values. As seen before we obtain the best agreement with data for rather low decoupling temperatures.

In conclusion, we observe that the coalescence mechanism is required to describe experimental data with our Langevin model. Only with the coalescence model is one able to describe both R_{AA} and v_2 consistently in the present model.

E. Dependence of the medium modification on the equation of state

The heavy flavor flow observables in Langevin simulations are quite sensitive to the description of the background medium used [24]. To examine this issue further, we have performed our calculations also using different equations of state that are implemented in the UrQMD hybrid model. Our results for different equations of state for the drag and diffusion coefficients of the resonance model with a decoupling temperature of 150 MeV are shown in Fig. 11 for the elliptic flow v_2 and for the nuclear modification factor R_{AA}.

We have used the chiral EoS for all results in the previous sections. It is constructed by matching a state-of-the-art hadronic chiral model to a mean-field description of the deconfined phase. The deconfinement transition in this approach is included by means of an effective Polyakov loop potential, coupling to the free quarks. It has been shown in [49] that the chiral EoS gives a reasonable description of lattice QCD thermodynamics at $\mu_B = 0$ and can be extended to finite baryon densities. The hadron resonance gas EoS resembles the active degrees of freedom, which are also included in the UrQMD transport approach, namely, most hadronic states and their resonances. The Bag model EoS [7] follows from matching a Walecka-type hadronic model to massless quarks and gluons via a Maxwell construction. It exhibits a strong first-order phase transition for all values of μ_B.

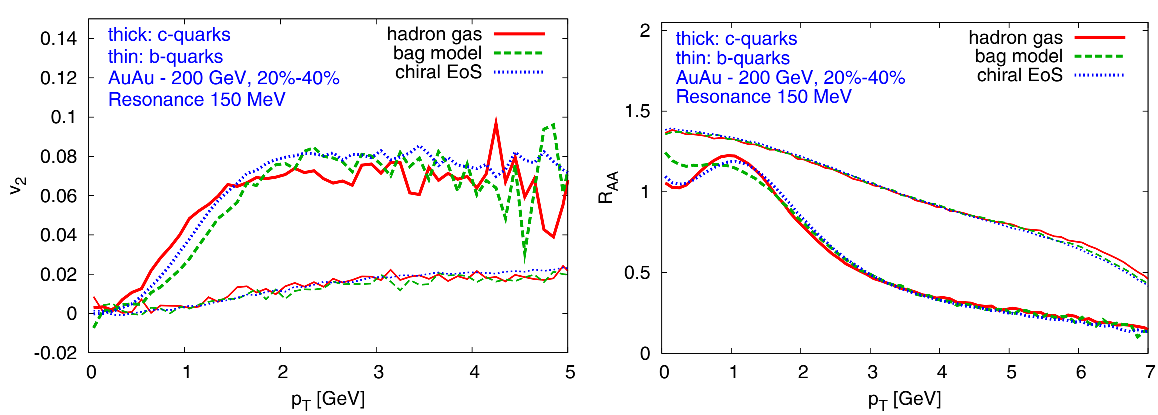

FIG. 11. Elliptic flow v_2 (left) and nuclear modification factor R_{AA} (right) of heavy quarks in Au + Au collisions at $\sqrt{s_{NN}} = 200$ GeV. We use a rapidity cutoff of $|y| < 0.35$. Different equations of state are compared.

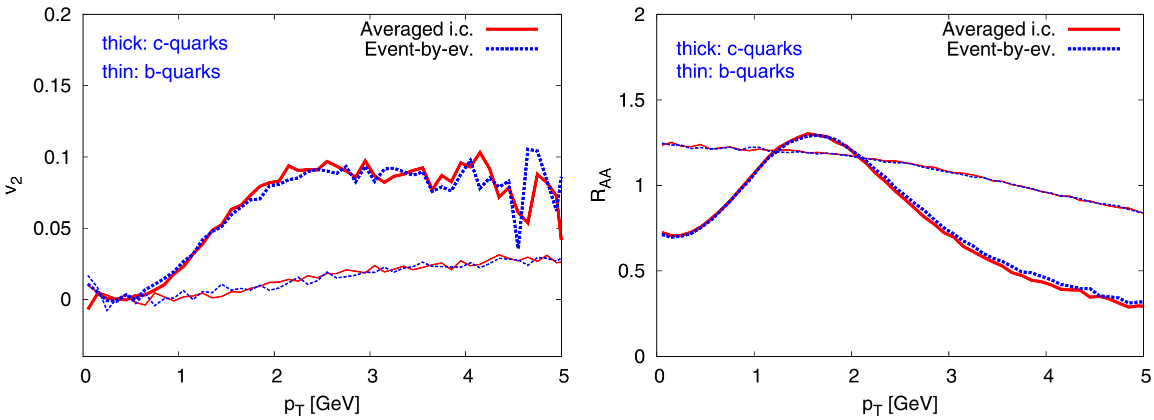

FIG. 12. Comparison between calculations with averaged initial conditions and calculations with fluctuating event-by-event initial conditions for the hydrodynamic stage. Left: Elliptic flow v_2 of heavy quarks in Au + Au collisions at $\sqrt{s_{NN}} = 200$ GeV. Right: Nuclear modification factor R_{AA} of heavy quarks in Au + Au collisions at $\sqrt{s_{NN}} = 200$ GeV. Parameters are $k = 1$ and $T_{\text{freeze-out}} = 150$ MeV.

As shown, clearly the influence on the medium's evolution as seen through the heavy quarks for this set of equations of state is very small.

F. Averaged initial condition vs fluctuating initial conditions

While it has long been known that the spatial energy density and entropy density distribution is strongly inhomogeneous in the initial state of a heavy ion collision [50], the influence of these inhomogeneities has only been studied systematically in recent years. However, an unambiguous answer whether fluctuating initial conditions (also known as event-by-event initial conditions) for the hydrodynamic stage of the simulation are really needed has become a long-standing debate. Previous studies have found that the difference between averaged and fluctuating initial conditions is usually small but depends on the observable under study (see, e.g., [51–56]).

For the present scenario we compare the results from fluctuating initial conditions vs averaged initial conditions in Fig. 12. For both heavy quark observables discussed here, i.e., elliptic flow and the nuclear modification factor, we observe only minuscule differences between averaged and fluctuating initial conditions.

V. RESULTS AT LHC ENERGIES

In the previous sections we found that we reach the best agreement with experimental PHENIX data when using the resonance model with a decoupling temperature of 130 MeV and using quark coalescence as the hadronization mechanism. Now we apply the same description also at LHC energies ($\sqrt{s_{NN}} = 2.76$ TeV). The momentum distribution for the initially produced charm quarks at the LHC is obtained from a fit to PYTHIA calculations. The fit function we use is

$$\frac{\mathrm{d}N}{\mathrm{d}^2 p_T} = \frac{1}{\left(1 + A_1 \cdot \left(p_T^2\right)^{A_2}\right)^{A_3}}, \tag{24}$$

with the coefficients $A_1 = 0.136$, $A_2 = 2.055$, and $A_3 = 2.862$.

We have performed our calculations in Pb + Pb collisions at $\sqrt{s_{NN}} = 2.76$ TeV in a centrality range of 30%–50%. The analysis is done with a rapidity cutoff of $|y| < 0.35$, in line with the ALICE data.

Figure 13 (left) depicts our results for elliptic flow compared to the ALICE measurements. The D-meson v_2 exhibits a strong increase and reaches a maximum at about $p_T = 3$ GeV, with $v_2 \sim 19\%$. The agreement between the ALICE measurements of D^0 and D^+ mesons and our calculation is quite satisfactory.

A complementary view on the drag and diffusion coefficients is provided by the nuclear suppression factor R_{AA}. Figure 13 (right) shows the calculated nuclear modification factor R_{AA} of D mesons at the LHC. In line with the experimental data the simulation is done for a more central bin of $\sigma/\sigma_{\text{tot}} = 0\%–20\%$. We find a maximum of R_{AA} at about $p_T = 2$ GeV, followed by a sharp decline to an R_{AA} of about 0.2 at high p_T. As shown we can describe the data well at medium p_T values but overpredict them at low-p_T bins.

VI. SUMMARY

In this paper we have investigated the medium modification of heavy quark p_T spectra in the hot medium created in heavy-ion collisions at RHIC and LHC energies based on a Langevin simulation for heavy quark diffusion in the QGP with hydrodynamical simulation of the "background medium" based on realistic initial conditions for both the bulk medium and the heavy quarks from the UrQMD transport model. The aim of this study was to find a consistent description for both the elliptic flow, v_2, and the nuclear modification factor, R_{AA}, with a realistic dynamical description of the background medium. We have used two sets of drag and diffusion coefficients, based on a T-matrix approach and a resonance-scattering model for the elastic scattering of heavy quarks with light quarks and antiquarks. Both sets of coefficients lead to similar results for the heavy flavor observables.

In the first part of our analysis we have used Peterson fragmentation to describe the hadronization of heavy quarks

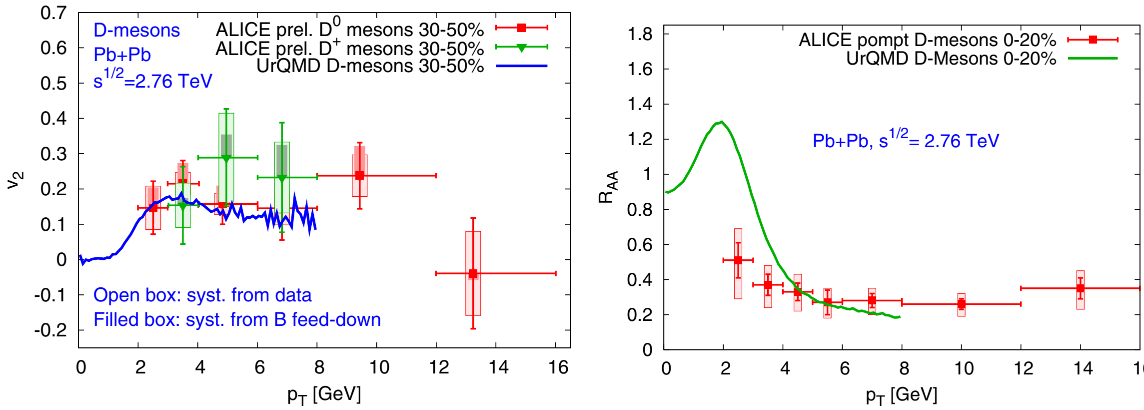

FIG. 13. Left: Flow v_2 of D mesons in Pb + Pb collisions at $\sqrt{s_{NN}} = 2.76$ TeV compared to data from the ALICE experiment [57]. A rapidity cutoff of $|y| < 0.35$ is employed. Right: R_{AA} of D mesons in Pb-Pb collisions at $\sqrt{s_{NN}} = 2.76$ TeV compared to experimental data from ALICE [58]. A rapidity cutoff of $|y| < 0.35$ is employed.

to open heavy flavor mesons. We have found a low elliptic flow and a too strong heavy flavor suppression at high p_T. Subsequently we have explored how a k factor for the drag and diffusion coefficients would influence the results. We found that with $k = 3$, the description of v_2 is improved, but there is an even larger suppression of the nuclear modification factor R_{AA}, as expected. We conclude that a combination of fragmentation and Langevin simulation with a k factor in the transport coefficient does not allow for a consistent description of the data on nonphotonic single-electron spectra in Au + Au collisions ($\sqrt{s_{NN}} = 200$ GeV) at the RHIC.

To overcome this problem we have used a coalescence approach to heavy quark hadronization to open heavy flavor mesons instead of fragmentation. The coalescence mechanism allows for a consistent description of both v_2 and R_{AA}. We have performed the simulations assuming different decoupling temperatures of heavy quarks from the medium and found that the late phase of the collision can have a considerable effect on the heavy quark observables. Within our study we find the best agreement with experimental data using the low decoupling temperature of 130 MeV. In Sec. IV E we have also addressed the sensitivity of the heavy flavor observables to the assumed EoS of the strongly interacting medium. Here we find that our results are insensitive to variations of the particular EoS used in the UrQMD hydrodynamic model. Also, fluctuations in the initial conditions, simulated with the UrQMD transport model, have an insignificant influence on the heavy quark observables.

Finally, we have also explored the medium modification in our model at LHC energies. Here we reached a good agreement with the data on the elliptic flow v_2 of D mesons. For the nuclear modification factor R_{AA} we reach a good agreement at medium p_T but seem to miss the data at low-p_T bins.

New complementary measurements with the STAR Heavy Flavor Tracker at $\sqrt{s_{NN}} = 200$ GeV are currently in progress. The Heavy Flavor Tracker will enable direct identification of heavy flavor meson decays like $D^0 \to K^-\pi^+$ and $D_s^+ \to K^-\pi^+K^+$. This is supposed to lead to better v_2 measurements down to very low p_T values and a better understanding of the energy loss of heavy quarks in the medium. Especially, it will provide us with identified D-meson spectra, which will enable us to compare our heavy meson results to data separately for D and B mesons and therefore to gain further insights into the hadronization mechanism.

ACKNOWLEDGMENTS

The authors thank P. B. Gossiaux, M. Nahrgang, and J. Aichelin for provision of the set of drag and diffusion coefficients derived by the Nantes group and H. Petersen for useful discussions about the simulations with averaged initial conditions. T. Lang and G. Inghirami gratefully acknowledge support from the Helmholtz Research School on Quark Matter Studies and from the Helmholtz Graduate School for Hadron and Ion Research. This work was supported by the Hessian LOEWE initiative through the Helmholtz International Center for FAIR (HIC for FAIR). J.S. acknowledges a Feodor Lynen fellowship from the Alexander von Humboldt Foundation. This work was supported by the Office of Nuclear Physics, U.S. Department of Energy's Office of Science, under Contract No. DE-AC02-05CH11231 and the Bundesministerium für Bildung und Forschung (BMBF) under Grant No. 06FY7083. Computational resources were provided by the Frankfurt LOEWE Center for Scientific Computing (LOEWE-CSC).

APPENDIX

1. Postpoint Ito realization

Since the phase-space distribution of relativistic particles is a scalar [59], the proper equilibrium limit is given by the corresponding boosted Boltzmann-Jüttner phase-space distribution,

$$f_Q^{(\mathrm{eq})} \propto \exp\left(-\frac{p \cdot u}{T}\right), \tag{A1}$$

where $u(t,\boldsymbol{x})$ is the four-velocity field of the medium and p the (on-shell) four-momentum of the heavy quark in the local rest frame. It can be shown analytically, and we have numerically checked, that to obey this constraint, one has to apply the postpoint prescription, $\xi = 1$, strictly only to the momentum argument of the covariance matrix C_{jk} as given in (7), and not to the corresponding coefficients originating from the Lorentz transformation of the time step $\mathrm{d}t$ with respect to the laboratory frame (plain symbols) to the one in the local rest frame of the heat bath (symbols with a superscript asterisk), i.e., in the transformation prescription for the time interval,

$$\mathrm{d}t^* = \frac{m}{E^*}\mathrm{d}\tau = \frac{m}{E^*}\frac{E}{m}\mathrm{d}t = \frac{E}{p\cdot u}\mathrm{d}t, \tag{A2}$$

one has to use the heavy quark momenta at time t without a postpoint update rule. Here, $\mathrm{d}\tau$ denotes the scalar "proper-time" interval of the heavy quark, corresponding to the given time interval, $\mathrm{d}t$, with respect to the laboratory frame [24].

2. Drag and diffusion coefficients I

We use two nonperturbative models for elastic heavy quark scattering in the QGP to evaluate the drag and diffusion coefficients for the Langevin simulation of heavy quark diffusion. The resonance model is based on heavy quark effective theory and chiral symmetry in the light quark sector [26]. Motivated by the finding in lattice-QCD calculations that hadron-like bound states and/or resonances might survive the phase transition in both the light-quark sector (e.g., ρ mesons) and heavy quarkonia (e.g., J/ψ), in this model we assume the existence of open heavy heavy flavor meson resonances like the D and B mesons.

In the T-matrix approach static in-medium quark-antiquark potentials from lattice QCD are used as scattering kernels in a Brückner-like T-matrix approach to calculate the scattering-matrix elements for elastic scattering of heavy quarks with light quarks and antiquarks [9]. The heavy-light quark resonance model [26] is based on the Lagrangian,

$$\begin{aligned}\mathscr{L}_{Dcq} = {}& \mathscr{L}_D^0 + \mathscr{L}_{c,q}^0 - \mathrm{i}G_S \\ &\times\left(\bar{q}\Phi_0^*\frac{1+\not{v}}{2}c - \bar{q}\gamma^5\Phi\frac{1+\not{v}}{2}c + \text{h.c.}\right) \\ &- G_V\left(\bar{q}\gamma^\mu\Phi_\mu^*\frac{1+\not{v}}{2}c - \bar{q}\gamma^5\gamma^\mu\Phi_{1\mu}\frac{1+\not{v}}{2}c + \text{h.c.}\right),\end{aligned} \tag{A3}$$

and an equivalent one for bottom quarks. Here v denotes the heavy quark four-velocity. The free part of the Lagrangian is given by

$$\begin{aligned}\mathscr{L}_{c,q}^0 &= \bar{c}(\mathrm{i}\not{\partial} - m_c)c + \bar{q}\,\mathrm{i}\not{\partial}q, \\ \mathscr{L}_D^0 &= (\partial_\mu\Phi^\dagger)(\partial^\mu\Phi) + (\partial_\mu{\Phi_0}^{*\dagger})(\partial^\mu\Phi_0^*) - m_S^2(\Phi^\dagger\Phi + \Phi_0^{*\dagger}\Phi_0^*) \\ &\quad - \tfrac{1}{2}(\Phi_{\mu\nu}^{*\dagger}\Phi^{*\mu\nu} + \Phi_{1\mu\nu}^\dagger\Phi_1^{\mu\nu}) + m_V^2(\Phi_\mu^{*\dagger}\Phi^{*\mu} + \Phi_{1\mu}^\dagger\Phi_1^\mu),\end{aligned} \tag{A4}$$

where Φ and Φ_0^* are pseudoscalar and scalar meson fields (corresponding to D and D_0^* mesons). Based on chiral symmetry, restored in the QGP phase, we also assume the existence of mass degenerate chiral-partner states. Farther from heavy quark effective symmetry one expects spin independence for both the masses, $m_S = m_V$, and the coupling constants, $G_S = G_V$. For the strange quark states we take into account only the pseudoscalar and vector states (D_s and D_s^*, respectively).

The D-meson propagators are dressed with the corresponding one-loop self-energy. Assuming charm and bottom quark masses of $m_c = 1.5$ GeV and $m_b = 4.5$ GeV, we adjust the masses of the physical D-meson-like resonances to $m_D = 2$ GeV and $m_B = 5$ GeV, in approximate agreement with the T-matrix models of heavy-light quark interactions in [60] and [61]. The coupling constant is chosen so as to obtain resonance widths of $\Gamma_{D,B} = 0.75$ GeV.

With these propagators the elastic Qq- and $Q\bar{q}$-scattering matrix elements are calculated and used for evaluation of the pertinent drag and diffusion coefficients for heavy quarks, using (A10) and (A11). It turns out that particularly the s-channel processes through a D/B-meson-like resonance provide a high efficiency for heavy quark diffusion compared to the pQCD cross sections for the same elastic scattering processes. This results in charm quark equilibration times $\tau_{\mathrm{eq}}^c = 2$–10 fm/c.

In order to justify the formation of D- and B-meson-like resonances above T_c, in [9] a Brueckner-like in-medium T-matrix approach has been used for the description of elastic heavy-light quark scattering in the QGP. After a three-dimensional reduction to a Lippmann-Schwinger equation, including a Breit correction, in-medium heavy quark potentials from lQCD have been employed as the scattering kernels. As an upper limit of the interaction strength within this approach,

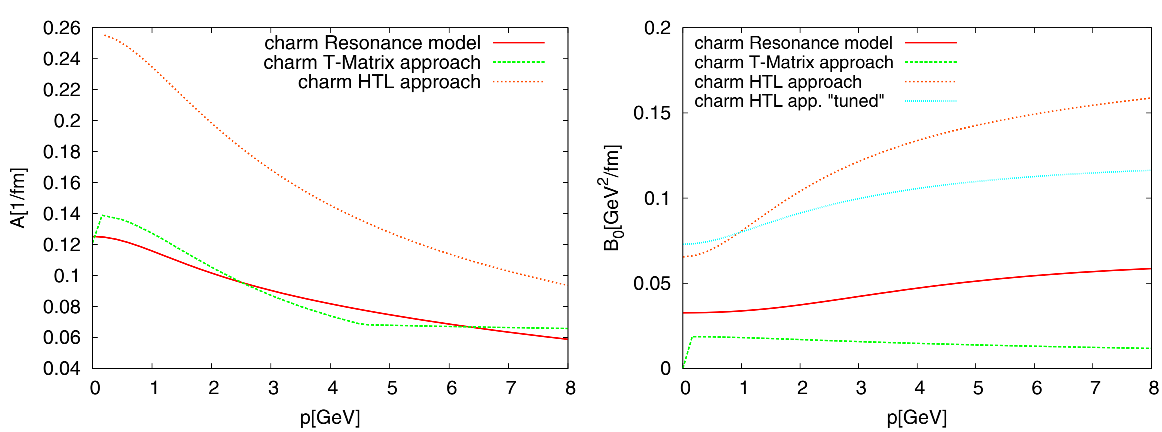

FIG. 14. Left: Comparison of the drag coefficients for charm quarks between the Nantes approach ("HTL") and our approach ("T-Matrix" and "Resonance"). Right: Comparison of the diffusion coefficients for charm quarks between the Nantes approach and our approach.

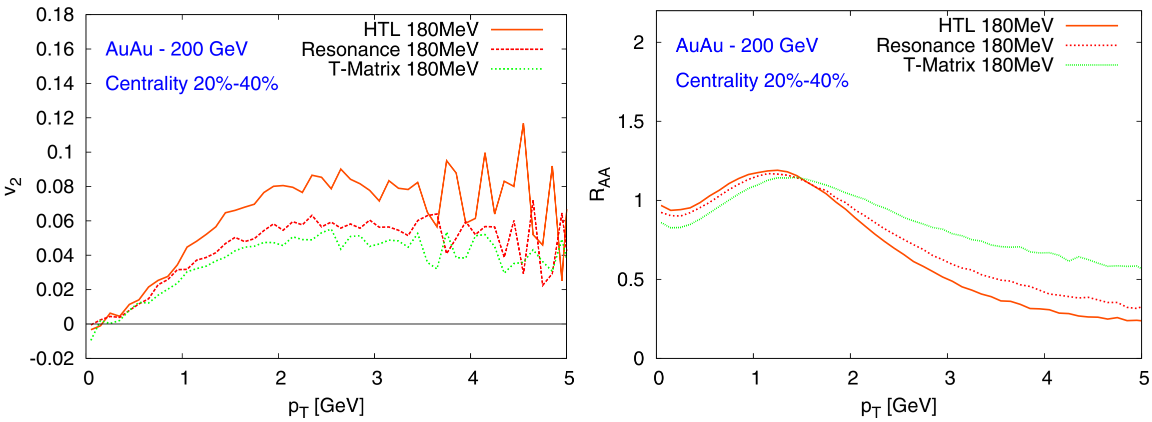

FIG. 15. Left: Comparison of the elliptic flows of charm quarks for different drag and diffusion coefficients. Right: Comparison of the nuclear modification factors of charm quarks for different drag and diffusion coefficients. As in all previous numerical simulations, even in this case the diffusion coefficients B_1 and B_0 are computed from the drag coefficient A using (21).

the internal-energy potential,

$$U(r,T) = F(r,T) - T\frac{\partial F(r,T)}{\partial T}, \tag{A5}$$

has been used, where F is the free-energy potential from the lattice calculation. We take into account also the complete set of $Q\bar{q}$ color states, assuming Casimir scaling of the corresponding potentials,

$$V_8 = -\tfrac{1}{8}V_1, \quad V_{\bar{3}} = \tfrac{1}{2}V_1, \quad V_6 = -\tfrac{1}{4}V_1. \tag{A6}$$

After a partial-wave decomposition the Lippmann-Schwinger equation,

$$T_{a,l}(E;q',q) = V_{a,l}(q',q) + \frac{2}{\pi}\int \mathrm{d}k k^2 V_{a,l}(q',k) G_{Qq}(E,k) \times T_{a,l}(E;k,q)\left[1 - f_F\left(\omega_k^Q\right) - f_F\left(\omega_k^q\right)\right], \tag{A7}$$

for the partial-wave components of each color channel, a, has been solved for the S- and P-wave components. Here, E is the center-of-momentum energy of the heavy-light quark system, q and q' the momenta of the heavy and light quarks, and

$$G_{qQ}(E,k) = \frac{1}{E - \left(\omega_k^q + \mathrm{i}\Sigma_I^q\right) - \left(\omega_k^Q + \mathrm{i}\Sigma_I^Q\right)} \tag{A8}$$

the corresponding two-particle propagator in the center-of-momentum frame. It has been checked that the quasiparticle widths of $\Gamma_I^{q,Q} = 2\Sigma_I^{q,Q} = 200$ MeV are consistent with a previous similar Brückner calculation [62] for light quarks and with the heavy quark self-energies with the T-matrix solution of (A7). The relation to the invariant scattering-matrix elements in (A10) is then given by

$$\sum |\mathcal{M}|^2 = \frac{64\pi}{s^2}\left(s - m_q^2 + m_Q^2\right)^2\left(s - m_Q^2 - m_q^2\right)^2 \times N_f \sum_a d_a\left(|T_{a,l=0}(s)|^2 + 3|T_{a,k=1}(s)\cos\theta_{\mathrm{cm}}|^2\right). \tag{A9}$$

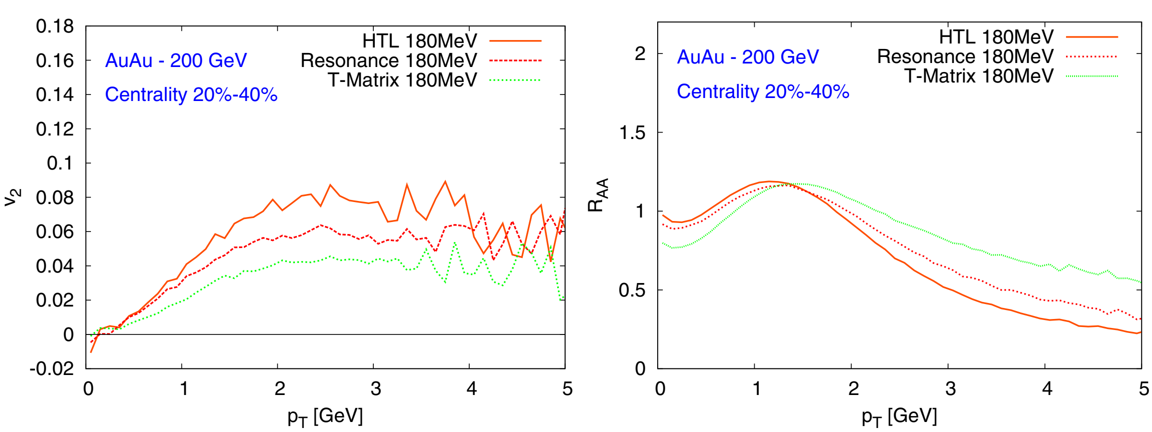

FIG. 16. Left: Comparison of the elliptic flows of charm quarks for different drag and diffusion coefficients. Right: Comparison of the nuclear modification factors of charm quarks for different drag and diffusion coefficients. In the numerical simulations performed to produce these plots, only the B_1 coefficients are computed from the A coefficients using (21), while the B_0 coefficients are taken from the underlying models for the HQ scattering cross sections.

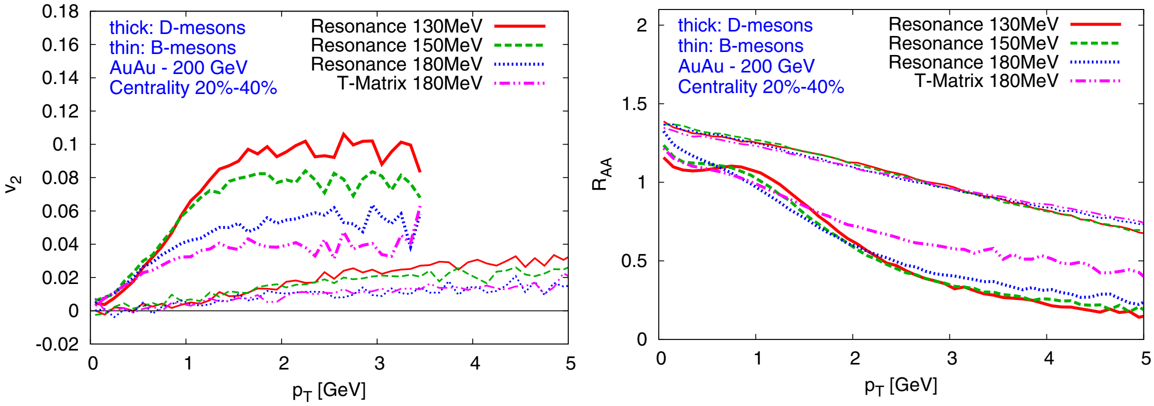

FIG. 17. Elliptic flow v_2 (left) and nuclear modification factor R_{AA} (right) of D and B mesons using Peterson fragmentation in Au + Au collisions at $\sqrt{s_{NN}} = 200$ GeV. We use a rapidity cutoff of $|y| < 0.35$.

The relation of elastic heavy quark scattering matrix elements to the drag and diffusion coefficients in the Langevin approach is given by integrals of the form

$$\begin{aligned}\langle X(\boldsymbol{p}')\rangle = {} & \frac{1}{2\omega_{\boldsymbol{p}}} \int_{\mathbb{R}^3} \frac{\mathrm{d}^3\boldsymbol{q}}{2E(\boldsymbol{q})(2\pi)^3} \int_{\mathbb{R}^3} \frac{\mathrm{d}^3\boldsymbol{p}'}{2E(\boldsymbol{p}')(2\pi)^3} \\ & \times \int_{\mathbb{R}^3} \frac{\mathrm{d}^3\boldsymbol{q}'}{2E(\boldsymbol{q}')(2\pi)^3} \frac{1}{\gamma_Q} \sum_{g,q} |\mathcal{M}|^2 \\ & \times (2\pi)^4 \delta^{(4)}(p+q-p'-q') f_{q,g}(\boldsymbol{q}) X(\boldsymbol{p}'). \end{aligned} \quad \text{(A10)}$$

Here, the integrations run over the three momenta of the incoming light quark or gluon, $\boldsymbol{q}$, and the momenta of the outgoing particles, $\boldsymbol{p}'$ and $\boldsymbol{q}'$. The sum over the matrix element is taken over the spin and color degrees of freedom of both the incoming and the outgoing particles; $\gamma_Q = 6$ is the corresponding spin-color degeneracy factor for the incoming heavy quark, and $f_{q,g}$ stands for the Boltzmann distribution function for the incoming light quark or gluon. In this notation, the drag and diffusion coefficients are given by

$$\begin{aligned} A(\boldsymbol{p}) &= \left\langle 1 - \frac{\boldsymbol{p}\boldsymbol{p}'}{\boldsymbol{p}^2} \right\rangle, \\ B_0(\boldsymbol{p}) &= \frac{1}{4}\left\langle \boldsymbol{p}'^2 - \frac{(\boldsymbol{p}'\boldsymbol{p})^2}{\boldsymbol{p}^2} \right\rangle, \\ B_1(\boldsymbol{p}) &= \frac{1}{2}\left\langle \frac{(\boldsymbol{p}'\boldsymbol{p})^2}{\boldsymbol{p}^2} - 2\boldsymbol{p}'\boldsymbol{p} + \boldsymbol{p}^2 \right\rangle, \end{aligned} \quad \text{(A11)}$$

with the angle bracket defined by the collision-integral functional (A10).

For both approaches we also include the leading-order perturbative QCD cross sections for elastic gluon heavy quark scattering [63], including a Debye screening mass $m_{Dg} = gT$ in the gluon propagators, thus taming the t-channel singularities in the matrix elements. The strong-coupling constant is chosen as $\alpha_s = g^2/(4\pi) = 0.4$.

3. Drag and diffusion coefficients II

The drag and diffusion coefficients employed in this study are taken from [9] and [27]. While the choice of these parameters is well justified, the choice is far from unique. To explore the differences and, possibly, the resulting systematic

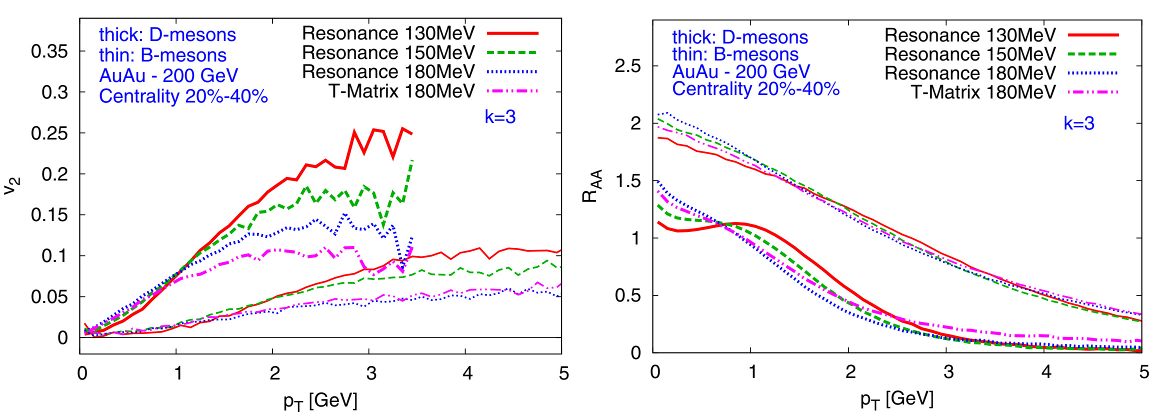

FIG. 18. Elliptic flow v_2 (left) and nuclear modification factor R_{AA} (right) of D and B mesons using Peterson fragmentation and a k factor of 3 in Au + Au collisions at $\sqrt{s_{NN}} = 200$ GeV. We use a rapidity cutoff of $|y| < 0.35$.

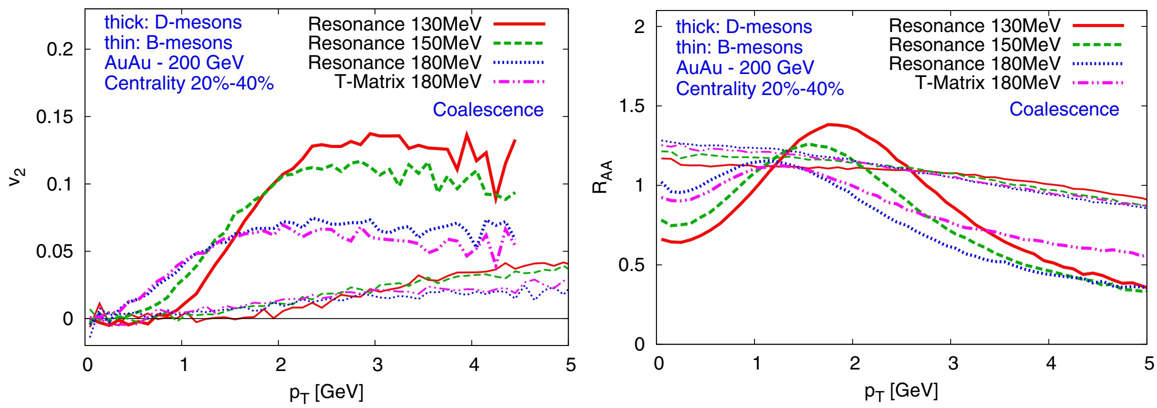

FIG. 19. Elliptic flow v_2 (left) and nuclear modification factor R_{AA} (right) of D and B mesons using coalescence in Au + Au collisions at $\sqrt{s_{NN}} = 200$ GeV. We use a rapidity cutoff of $|y| < 0.35$.

uncertainties in the observables, we compare the coefficients employed here with the drag and diffusion coefficients derived by the Nantes group (see, e.g., [64]).

Figure 14 shows the comparison between the Nantes coefficients (labeled "HTL") and the coefficients used in the rest of the article, labeled "Resonance" and "T-matrix." Here HTL indicates the Nantes coefficients calculated following the definition in [35], while "HTL tuned" corresponds to some tuning of the B_1 and B_0 coefficients in order to assure that the asymptotic distribution corresponds to Boltzmann-Jüttner (A is not tuned and is kept as is) (for details see Ref. [65]). The figures indicate that the differences between the drag and the diffusion coefficients are substantial (on average more than a factor of 2) over all charm momenta.

Let us now compare how these differences influence the finally observed D-meson elliptic flow and the nuclear modification factor (Fig. 15). In our numerical simulations we used the HTL coefficients without any tuning, since the tuned ones were computed only up to temperatures of 400 MeV. Figure 16 shows the comparison in detail.

4. Underlying D- and B-meson spectra before semileptonic decays

The heavy flavor electron spectra at the RHIC originate from D- and B-meson decays. These D- and B-meson spectra are obtained from our heavy quark calculations applying a fragmentation or a coalescence mechanism. They are displayed in Fig. 17 for the case of Peterson fragmentation without using a k factor, in Fig. 18 for the case of Peterson fragmentation applying a k factor of 3, and, finally, for the case of using a coalescence mechanism (Fig. 19).

These spectra can act as a prediction for future D- and B-meson measurements at RHIC energies. They allow, on the one hand, for a comparison of our hadronization mechanisms with experimental data and, on the other hand, for a comparison of the decay to heavy flavor electrons performed using PYTHIA.

[1] J. Adams *et al.* (STAR Collaboration), Nucl. Phys. A **757**, 102 (2005).
[2] K. Adcox *et al.* (PHENIX Collaboration), Nucl. Phys. A **757**, 184 (2005).
[3] B. Müller, J. Schukraft, and B. Wyslouch, Annu. Rev. Nucl. Part. Sci. **62**, 361 (2012).
[4] S. Bass, M. Belkacem, M. Bleicher, M. Brandstetter, L. Bravina *et al.*, Prog. Part. Nucl. Phys. **41**, 255 (1998).
[5] M. Bleicher, E. Zabrodin, C. Spieles, S. Bass, C. Ernst *et al.*, J. Phys. G **25**, 1859 (1999).
[6] D. H. Rischke, S. Bernard, and J. A. Maruhn, Nucl. Phys. A **595**, 346 (1995).
[7] D. H. Rischke, Y. Pursun, and J. A. Maruhn, Nucl. Phys. A **595**, 383 (1995).
[8] R. Rapp and H. van Hees, in *Quark Gluon Plasma 4*, edited by R. C. Hwa and X.-N. Wang (World Scientific, Singapore, 2009), p. 111.
[9] H. van Hees, M. Mannarelli, V. Greco, and R. Rapp, Phys. Rev. Lett. **100**, 192301 (2008).
[10] H. van Hees, V. Greco, and R. Rapp, J. Phys. G **35**, 125 (2008).
[11] V. Greco, H. van Hees, and R. Rapp, arXiv:0709.4452 [hep-ph].
[12] H. van Hees, M. Mannarelli, V. Greco, and R. Rapp, Eur. Phys. J. **61**, 799 (2009).
[13] R. Rapp, D. Cabrera, V. Greco, M. Mannarelli, and H. van Hees, arXiv:0806.3341 [hep-ph].
[14] R. Rapp and H. van Hees, in *The Physics of Quarks: New Research. Horizons in World Physics*, Vol. 265 (Nova Science, Hauppauge, NY, 2009).
[15] M. He, R. J. Fries, and R. Rapp, Phys. Rev. Lett. **110**, 112301 (2013).
[16] M. He, R. J. Fries, and R. Rapp, Nucl. Phys. A **910–911**, 409 (2013).
[17] J. Aichelin, P. B. Gossiaux, and T. Gousset, Acta Phys. Polon. B **43**, 655 (2012).
[18] J. Uphoff, O. Fochler, Z. Xu, and C. Greiner, Phys. Rev. C **84**, 024908 (2011).
[19] J. Uphoff, O. Fochler, Z. Xu, and C. Greiner, Phys. Lett. B **717**, 430 (2012).
[20] C. Young, B. Schenke, S. Jeon, and C. Gale, Phys. Rev. C **86**, 034905 (2012).
[21] G. D. Moore and D. Teaney, Phys. Rev. C **71**, 064904 (2005).
[22] I. Vitev, A. Adil, and H. van Hees, J. Phys. G **34**, S769 (2007).

[23] P. Gossiaux, J. Aichelin, T. Gousset, and V. Guiho, J. Phys. G **37**, 094019 (2010).
[24] P. B. Gossiaux, S. Vogel, H. van Hees, J. Aichelin, R. Rapp, M. He, and M. Bluhm, arXiv:1102.1114 [hep-ph] (2011).
[25] P. Gossiaux, J. Aichelin, and T. Gousset, Prog. Theor. Phys. Suppl. **193**, 110 (2012).
[26] H. van Hees and R. Rapp, Phys. Rev. C **71**, 034907 (2005).
[27] H. van Hees, V. Greco, and R. Rapp, Phys. Rev. C **73**, 034913 (2006).
[28] H. Petersen, J. Steinheimer, G. Burau, M. Bleicher, and H. Stöcker, Phys. Rev. C **78**, 044901 (2008).
[29] J. Steinheimer, M. Bleicher, H. Petersen, S. Schramm, H. Stöcker, and D. Zschiesche, Phys. Rev. C **77**, 034901 (2008).
[30] H. Petersen, C. Coleman-Smith, S. A. Bass, and R. Wolpert, J. Phys. G **38**, 045102 (2011).
[31] Q. Li, J. Steinheimer, H. Petersen, M. Bleicher, and H. Stöcker, Phys. Lett. B **674**, 111 (2009).
[32] F. Cooper and G. Frye, Phys. Rev. D **10**, 186 (1974).
[33] P. Huovinen and H. Petersen, Eur. Phys. J. A **48**, 171 (2012).
[34] B. Svetitsky, Phys. Rev. D **37**, 2484 (1988).
[35] M. G. Mustafa, D. Pal, and D. K. Srivastava, Phys. Rev. C **57**, 889 (1998).
[36] P. B. Gossiaux and J. Aichelin, Phys. Rev. C **78**, 014904 (2008).
[37] P. B. Arnold, Phys. Rev. E **61**, 6091 (2000).
[38] M. He, H. van Hees, P. B. Gossiaux, R. J. Fries, and R. Rapp, Phys. Rev. E **88**, 032138 (2013).
[39] J. Dunkel and P. Hänggi, Phys. Rep. **471**, 1 (2009).
[40] R. Rapp, V. Greco, and H. van Hees, Nucl. Phys. A **774**, 685 (2006).
[41] M. He, R. J. Fries, and R. Rapp, Phys. Lett. B **701**, 445 (2011).
[42] P. Huovinen, P. Kolb, U. W. Heinz, P. Ruuskanen, and S. Voloshin, Phys. Lett. B **503**, 58 (2001).
[43] D. Krieg and M. Bleicher, Eur. Phys. J. A **39**, 1 (2009).
[44] C. Peterson, D. Schlatter, I. Schmitt, and P. M. Zerwas, Phys. Rev. D **27**, 105 (1983).
[45] J. Chrin, Z. Phys. C **36**, 163 (1987).
[46] T. Sjostrand, S. Mrenna, and P. Z. Skands, J. High Energy Phys. 05 (2006) 026.
[47] T. Sjostrand, S. Mrenna, and P. Z. Skands, Comput. Phys. Commun. **178**, 852 (2008).
[48] A. Adare *et al.* (PHENIX Collaboration), Phys. Rev. C **84**, 044905 (2011).
[49] J. Steinheimer, S. Schramm, and H. Stöcker, Phys. Rev. C **84**, 045208 (2011).
[50] M. Bleicher, L. Gerland, C. Spieles, A. Dumitru, S. Bass *et al.*, Nucl. Phys. A **638**, 391c (1998).
[51] H.-J. Drescher and Y. Nara, Phys. Rev. C **76**, 041903 (2007).
[52] B. Tavares, H.-J. Drescher, and T. Kodama, Braz. J. Phys. **37**, 41 (2007).
[53] R. Andrade, A. dos Reis, F. Grassi, Y. Hama, W. Qian, and T. Kodama, Acta Phys. Polon. B **40**, 931 (2009).
[54] R. P. G. Andrade, F. Grassi, Y. Hama, T. Kodama, and W. L. Qian, Phys. Rev. Lett. **101**, 112301 (2008).
[55] H. Petersen and M. Bleicher, Phys. Rev. C **79**, 054904 (2009).
[56] H. Petersen and M. Bleicher, Phys. Rev. C **81**, 044906 (2010).
[57] Z. C. del Valle, Nucl. Phys. A **904–905**, 178c (2013).
[58] B. Abelev *et al.* (ALICE Collaboration), J. High Energy Phys. 09 (2012) 112.
[59] S. R. de Groot, W. A. van Leeuwen, and C. G. van Weert, *Relativistic Kinetic Theory: Principles and Applications* (North-Holland, Amsterdam, 1980).
[60] D. Blaschke, G. Burau, T. Barnes, Y. Kalinovsky, and E. Swanson, Heavy Ion Phys. **18**, 49 (2003).
[61] D. Blaschke, G. Burau, Y. L. Kalinovsky, and V. L. Yudichev, Prog. Theor. Phys. Suppl. **149**, 182 (2003).
[62] M. Mannarelli and R. Rapp, Phys. Rev. C **72**, 064905 (2005).
[63] B. L. Combridge, Nucl. Phys. B **151**, 429 (1979).
[64] M. Nahrgang, J. Aichelin, P. B. Gossiaux, and K. Werner, Phys. Rev. C **90**, 024907 (2014).
[65] P. B. Gossiaux, V. Guiho, and J. Aichelin, J. Phys. G **31**, S1079 (2005).